Geoacoustic inversion of reflection loss data

Leif Abrahamsson
Brodd Leif Andersson
Stefan Ban
Eva Dalberg
Per Söderberg

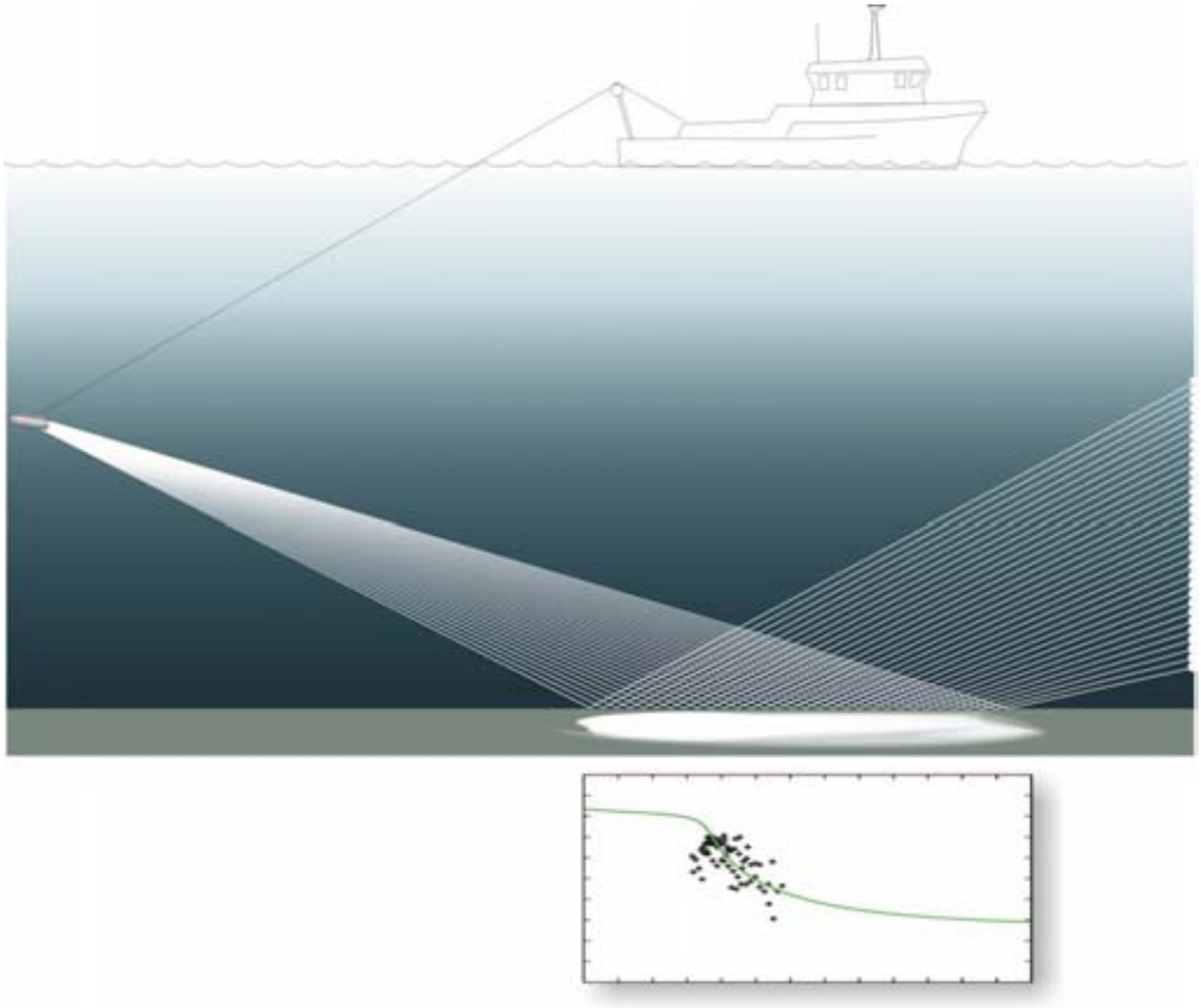

FOI-R--1726--SE
ISSN 1650-1942

Systems Technology
Technical report

October 2005

Geoacoustic inversion of reflection loss data

FOI-R--1726--SE
ISSN 1650-1942

Systems Technology
Technical report

October 2005

Issuing organization	Report number, ISRN	Report type
FOI – Swedish Defence Research Agency Systems Technology SE-164 90 Stockholm	FOI-R--1726--SE	Technical report
	Research area code 4. C4ISTAR	
	Month year October 2005	**Project no.** E60703
	Sub area code 43 Underwater Surveillance, Target acquistion and Reconnaissance	
	Sub area code 2	

Author/s (editor/s)	Project manager
Leif Abrahamsson Brodd Leif Andersson Stefan Ban Eva Dalberg Per Söderberg	Peter Krylstedt
	Approved by Monica Dahlén
	Sponsoring agency Swedish Armed Forces
	Scientifically and technically responsible Leif Abrahamsson

Report title

Geoacoustic inversion of reflection loss data

Abstract

This report presents a fast inversion technique to determine the sound velocity of the topmost sediment layer using broadband reflection loss data in the frequency range 0.5-4 kHz. The measurements of bottom reflections were performed in June 2005 at a test site with a sandy bottom. The acoustic signals were transmitted by a moving source which was allowed to pass a vertical receiver array at close distance. The measured bottom reflections at different angles of incidence towards the bottom were compared to model calculations based on the Rayleigh model of plane wave reflections. A best fit between computed and measured reflection loss data is sought by using an inversion scheme in which different sets of bottom parameters are tried. The inversion results show that the velocity of the sediment at the test site varies between 1480 to 1700 m/s. A computationally intensive full-field model was used to check the accuracy of the Rayleigh model.

The run time of an inversion amounts to a few seconds. It implies that the proposed technique can be used in real-time for inversions of data collected on moving platforms.

This work is part of an ongoing development of operational techniques for REA (Rapid Environmental Assessment).

Keywords

key words: underwater acoustics, inversion, bottom reflections, Rayleigh model

Further bibliographic information	Language English

ISSN 1650-1942	Pages 28 p.
	Price acc. to pricelist

Utgivare FOI - Totalförsvarets forskningsinstitut Systemteknik 164 90 Stockholm	**Rapportnummer, ISRN** FOI-R--1726--SE	**Klassificering** Teknisk rapport
	Forskningsområde 4. Ledning, informationsteknik och sensorer	
	Månad, år Oktober 2005	**Projektnummer** E60703
	Delområde 43 Undervattenssensorer	
	Delområde 2	

Författare/redaktör Leif Abrahamsson Brodd Leif Andersson Stefan Ban Eva Dalberg Per Söderberg	**Projektledare** Peter Krylstedt
	Godkänd av Monica Dahlén
	Uppdragsgivare/kundbeteckning Försvarsmakten
	Tekniskt och/eller vetenskapligt ansvarig Leif Abrahamsson

Rapportens titel (i översättning)

Geoakustisk inversion av reflektionsförlustdata

Sammanfattning

I denna rapport redovisas en snabb inversionsteknik för att bestämma ljudhastigheten i det övre sedimentskiktet med hjälp av bredbandiga reflektionsförlustdata i frekvensområdet 0.5-4 kHz. Mätningarna av bottenreflektioner utfördes i juni 2005 i ett försöksområde med sandbotten. De akustiska signalerna sändes ut från en rörlig källa som fick passera en vertikal mottagararray på nära avstånd. De uppmätta bottenreflektionerna jämfördes med modellberäkningar baserade på planvågsreflektioner enligt Rayleighmodellen. I inversionen söker man en bästa anpassning mellan beräknade och uppmätta reflektionsförlustadata genom att prova olika uppsättningar av bottenparametrar. Inversionsresultaten visar att ljudhastigheten hos sedimentet på mätplatsen varierar mellan 1480 och 1700 m/s. En beräkningsintensiv fullfältsmodell användes för att kontrollera noggrannheten av Rayleighmodellen.

Inversionsberäkningarna kunde utföras på några sekunder. Det innebär att den föreslagna tekniken kan användas i realtid för inversion av data som samlats in på rörliga plattformar.

Detta arbete är ett led i en pågående utveckling av operationella metoder för REA (Rapid Environment Assessment).

Nyckelord

undervattensakustik, inversion, bottenreflektioner, Rayleighmodell

Övriga bibliografiska uppgifter	**Språk** Engelska
ISSN 1650-1942	**Antal sidor:** 28 s.
Distribution enligt missiv	**Pris: Enligt prislista**

Contents

1 Introduction

The variability of the sea and the seabed as acoustic media is a major concern in the navy as it affects the performance of sonar systems for ASW and MCM. Environment data bases are helpful, but occasionally they are deficit or inaccurate. For example, the sound velocity of the surficial sea water may change in the course of a day and significantly depart from the average distribution for the season of the year. Another factor of importance is seabed type. Here there are geographical areas where acoustic parameters of the bottom are poorly known. Yet they are part of the input to sonar decision support systems for prediction of detection ranges [1], [2].

This report presents results from an experiment directed towards operational REA (Rapid Environment Assessment). The objective is to develop fast techniques to determine acoustic bottom parameters. In the experiment three types of broadband acoustic data were collected: reflection loss, reverberation and transmission loss data. The results presented in this paper concern only the reflection loss measurements. The inversion is based on model-data comparisons using the Rayleigh model of plane wave reflections of layered media. This approach enables a quick estimate of the sound velocity of the topmost sediment. The emphasis of this study is on the modeling aspects of fast geoacoustic inversion techniques. A selection of measurements are used for testing and evaluation of the proposed methods. The inversion results show that the sound velocity of the sediment at the test site varies between 1480 and 1750 m/s. The run time of such inversions amounts to a few seconds. The fast computational speed makes it possible to apply the technique to real-time inversions of reflection loss data collected on moving platforms.

The present study of the reflectivity of the bottom is part of a series of experiments, the aim of which is to isolate and quantify bottom parameters of crucial importance to sound propagation in the frequency band 0.5-4 kHz. Measurements of the reflection coefficient of the direct bottom bounce are suitable for inversion of the velocity of the surficial sediment. Reverberation data primarily provides information of the scattering strength of the bottom. Both of these measurements were made at short source-receiver distances and are applicable to active sonar with towed array receivers. The transmission loss measurements were made with chirp signals at nearly fixed ranges 0.5, 1, 2 and 4 km. As opposed to the previous cases, this configuration requires one platform for transmission and another one for reception. On the other hand it enables transmission of probing signals over propagation distances of most interest for target detection. The analysis of the reverberation and transmission loss data will be reported elsewhere as well as the related topic on how to combine short and long range inversions. These issues are addressed on research on low frequency active sonar [3], [4]. The basic idea is to exploit the operational sonar for bottom characterization as a complement to environmental data bases. The requirement of fast run times during the conduct of constrained missions at sea often implies that fewer parameters are being inverted for than in carefully controlled experiments.

2 The field trial

2.1 The test site

2.1.1 Geological background

The sea tests took place in the beginning of June 2005 a few km SE of Nynäshamn, in the vicinity of a small island.

The bedrock of this part of the archipelago consists mainly of crystalline granites, gneisses and leptites formed about 1800 Ma ago. The area is intersected by tectonic lineaments and fracture zones, in part very deep, which contribute to the large extension of the archipelago. These structures where at least partly initiated in connection with the bedrock formation and have been reactivated several times since then.

In general the bedrock is covered by unconsolidated sediments which may be generalised as follows; A thin layer of till is covering the bedrock, typically some metres thick. On top of the till are glacial and post glacial clays deposited. Typically, the glacial clay is quite uniform in thickness being frequently a few metres thick. The glacial deposits are succeeded by post glacial clays and recent mud. The thickness of these sediments is highly variable due to local variations in condition of accumulation and erosion. Locally the post glacial sediment amounts to several tens of metres in thickness.

As the area is affected by the Middle Swedish Icemarginal Zone the sediments in the test area are more sandy/gravely than the mean part of the archipelago. The icemarginal sediments are composed og glacigenic, waterlain sediments, consisting of well-washed and sorted beds of sand and gravel and poorly sorted till layers.

Due to the ongoing land upheaval together with other acting agents the upper sediment layer/layers may locally consist of sand redeposited on top of clay. This is at least valid for the near shore areas wheras the deeper parts mostly consists of post glacial clay.

2.1.2 The sound speed profile

At the time of the experiment the sound velocity of the surficial sea water may vary hour by hour due to sun-heating and water mixing by wave action. The fluctuations are exemplified in Fig. 2.1, which shows a number of sound speed profiles measured at various places near the receiver array during a short period of time.

The measured profiles often exhibit small-scale oscillations of random nature which are neglible for wave propagation at frequencies less than a few kHz. Therefore it is common practice in modeling work to downsample and smooth the measured profiles. Figure 2.2 shows a smoothed adjustment (red curve) of the measured profile (black) being used in this report.

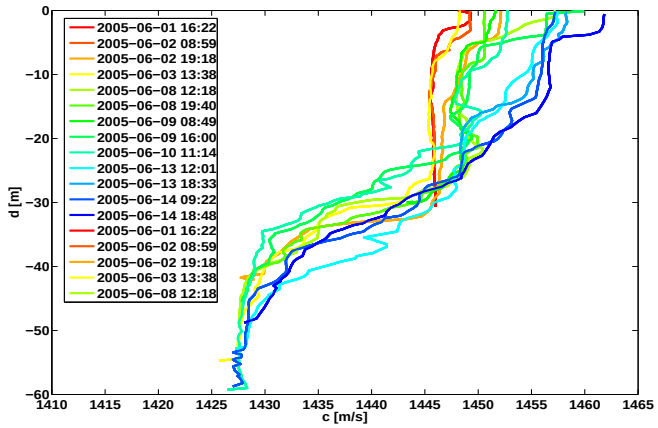

Figure 2.1: *Samples of sound velocity profiles measured in June 2005.*

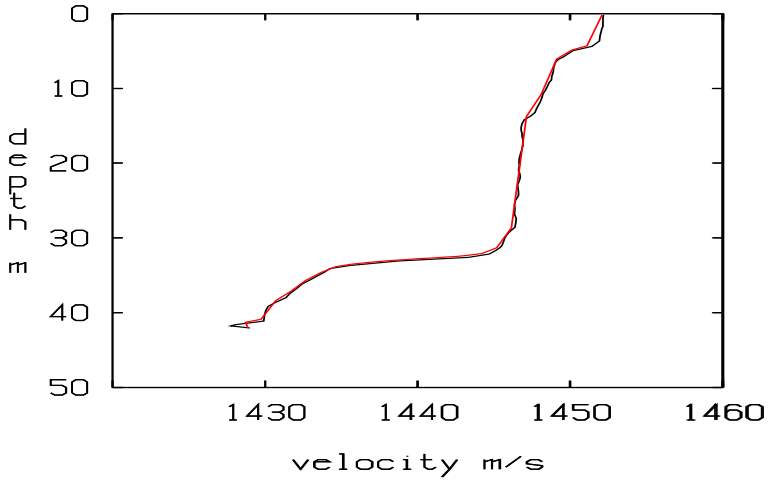

Figure 2.2: *The measured (black) and smoothed (red) sound speed profiles being used in this report.*

2.2 Experimental setup

The measurement system consisted of a transmitter unit, a vertical receiver array, and two data acquisition systems. The transmitter unit consisted of an Argotec transducer model 215 with a maximum source level of 164 dB re 1 μPa at 1 m, and a reference hydrophone. The transmitter and the reference hydrophone were mounted on a metal assembly with the hydrophone in a free-hanging position 0.8 m ahead of the transmitter. The transmitter unit was operated from the research vessel HMS Ägir. For the reflection loss measurements the ship was maneuvered near the receiver array while the transmitter unit was lowered to the depth 15.5 m. Just prior to the transmissions the engines were turned off and the ship was drifting and towing the transmitter unit towards and away from the receiver. The drift velocity was around 0.5 m/s. Four repeated runs were made in various directions on which the distance between the source and receiver ranged from 10 to 150 m. The tracks, denoted by 1, 2, 3 and 4, are shown in Fig. 2.3. The signal from the reference hydrophone was sampled at 40 kHz and

recorded along with time information on a 2-channel recorder aboard HMS Ägir.

The 31-element vertical receiver array was bottom moored at a water depth of 27 m. The array spanned water depths from 10 to 26.5 m. The separation distance between the hydrophones was 0.5 m except for the 1st and 2nd, and the 15th and 16th (counted from the top), which were spaced by 1 and 1.5 m respectively. Hydrophones no 8 and 14 were calibrated before the trial with a sensitivity of -136 dB re $1V/\mu Pa$ and with a flat frequency response in the range of interest. The array was connected by a cable to the data acquisition system on a nearby island. The received signals were amplified, filtered (20 Hz - 5 kHz), and digitized by a 32-channel 16 bit data acquisition system with a sampling frequency of 40 kHz. One of the channels was reserved for time recordings (IRIG-B) to be used for time synchronization with the transmitter unit.

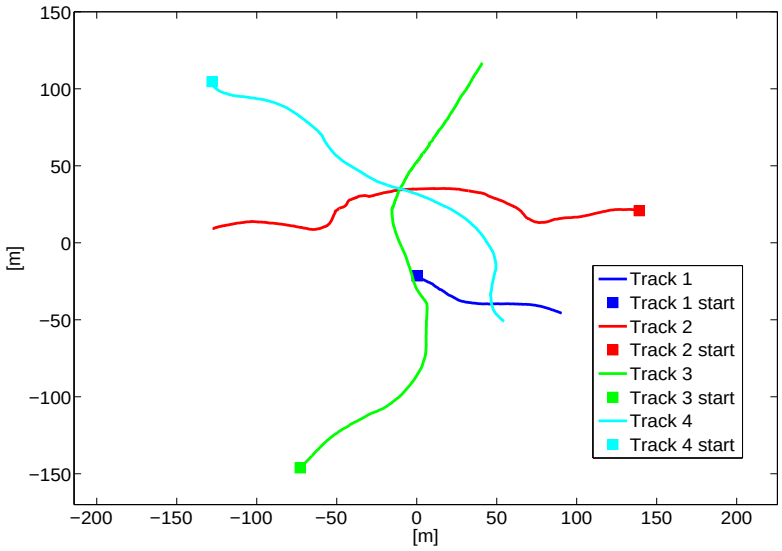

Figure 2.3: *Traces relative the receiver postion at (0,0) of the drifting ship as it was towing the transmitter. The four tracks will be denoted by 1 (blue), 2 (red), 3 (green) and 4 (lightblue).*

2.3 Transmitted waveforms

Two types of broadband pulses, Ricker pulses and Ricker chirps, were used in the experiment. The Ricker pulses will be denoted by $r_a[f_c]$, where f_c $[kHz]$ is the center frequency of the pulse. The center frequency f_c is a free parameter that controls the pulse length ($\approx 1.2 f_c^{-1}$ $[ms]$) or the bandwidth. The subindex $'a'$ refers to the fact that $r_a[f_c]$ is the autocorrelation of the original Ricker pulse. Four Ricker pulses with the center frequencies 0.5, 1, 2, and 4 kHz were used. The Ricker chirp, denoted by $r_c[f_c, T]$, is an amplitude and frequency modulated pulse. It has two free parameters f_c, T $[kHz, ms]$ for selection of bandwidth and pulse length. The autocorrelation of the Ricker chirp $r_c[f_c, T]$ is practically identical to $r_a[f_c]$ for arbitrary choices of T. The

following Ricker chirps were transmitted:

$$r_c[0.5, 120] \qquad r_c[1, 60] \qquad r_c[2, 30] \qquad r_c[4, 15]. \tag{2.1}$$

The waveforms of $r_c[1, 60]$ and $r_a[1]$ are displayed in Fig. 2.4. The 0.5, 2 and 4 kHz pulses are obtained by a change of scale of the time variable with a factor of 2, 1/2 and 1/4 respectively. The time resolution is 0.3, 0.6, 1.2 and 2.4 ms for f_c= 4, 2, 1 and 0.5 kHz respectively. The corresponding spatial resolution is 0.45, 0.9, 1.8 and 3.6 m. Analytic expressions, as well as an account of the properties of these pulses, are given in [5].

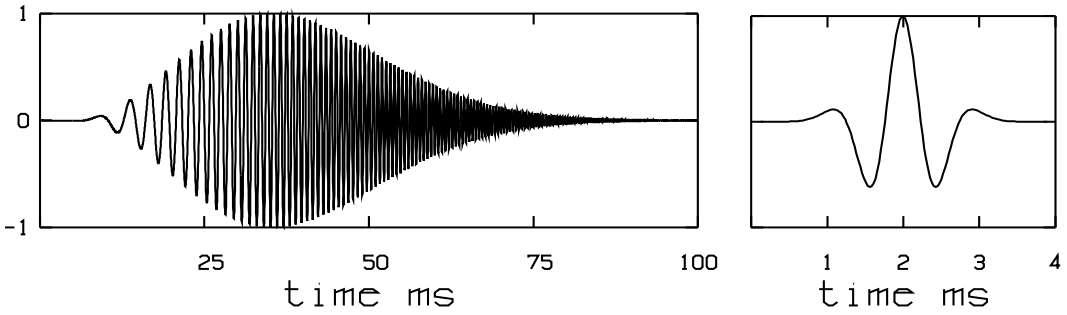

Figure 2.4: *The two 1 kHz pulses being used in the experiment,* $r_c[1, 60]$ *(left) and its autocorrelation* $r_a[1]$*(right)*

The autocorrelation relationship between the pulses makes it possible to assess the effect of noise reduction by matched filtering by a direct comparison. The improvement of the signal-to-noise ratio (SNR) amounts to $10 log BT$ $[dB]$, where BT is the time-bandwidth product. If B and T are evaluated by formulas for effective values of the widths in frequency and time, the expected gain is 16 dB for all four Ricker chirps after matched filtering.

Source excitation by Ricker chirps and pulses in model computations gives identical solutions after crosscorrelation of the Ricker chirp solution with the source pulse. This equivalence can be expoited to enhance computational efficiency when time domain solutions are synthesized using transfer functions. Since the size of the required transform (FFT) is much smaller for the Ricker pulse, because of its shorter duration, it should be substituted in model computations with chirp signals.

The eight signals were transmitted in a sequence 0.5 s apart comprising a recording time of 4 s. The 4-s pulse block was repeated without time gaps as the track was traversed. For a drift speed around 0.5 m/s, the separation distance between pings of the same pulse was around 2 m.

2.4 Data processing

The received raw signals from the chirp transmissions were crosscorrelated with the corresponding synthetic source pulse. The correlation output was normalized by the energy integral of the source pulse, which makes the filtering process neutral with respect to signal amplitude while noise components are suppressed. The measured time series from the transmissions of the Ricker pulses were bandpass filtered with passbands equal to the effective bandwidth ($\approx 0.8 f_c$). Figure 2.5 shows the 4-kHz synthetic signals as well as the raw and filtered signals at the reference hydrophone.

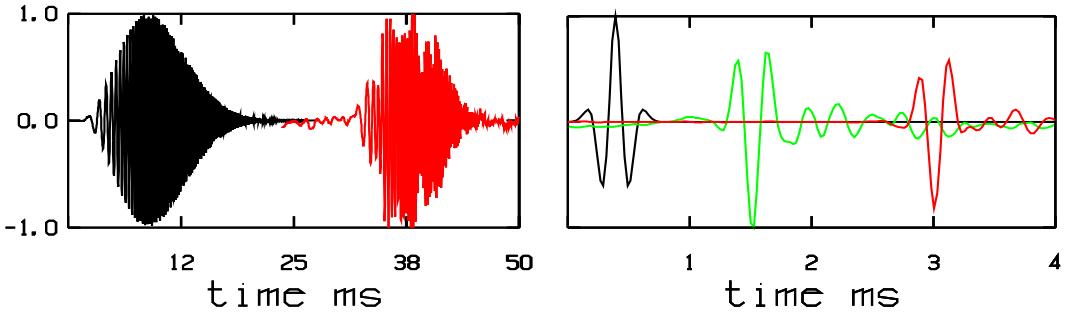

Figure 2.5: *Left: the synthethic Ricker chirp (black) and the response at the the reference hydrophone (red). Right: the synthetic Ricker pulse (black), its response at the reference hydrophone (green) and the matched filtered Ricker chirp (red), which is the crosscorrelation of the two signals in the left panel.*

The waveforms of the filtered Ricker pulse (green) and the matched filtered chirp signal (red) displayed at the right panel of Fig. 2.5 are practically identical as expected. The discrepancies between the received waveforms and the synthetic driver signals are less at the receiver array, although some source ringings persist, see Figs. 2.6 and 2.7 below. However the distortions at the reference hydrophone did not preclude an accurate determination of the arrival time of the peak of the pulse. This instant, corrected for the travel time between the transmitter and the reference hydrophone, establishes the time when the peak of the pulse leaves the transmitter. This time is taken as the initial time in extracting each ping at the receiver recordings for output on a separate file. The next processing step is to determine the horizontal distance between the source and the receiver array. It was obtained by searching for the arrival time of the peak of the direct wave at hydrophone no 11, which was located at the same depth as the transmitter. This task was accomplished in two steps. First the initial rise of the peak of the direct wave was identified by the first occurrence when the energy amplitude exceeded the background level by 10 dB. After that a time-window commensurate with the pulse length was placed around this point and searched for the peak amplitude. Although this approach was not entirely faultless, it turned out to be more robust then using correlation techniques for identification of the direct arrival. Throughout this report signal levels of direct arrivals, surface and bottom echoes are based on peak values of the envelope squared of the signal. Attempts to use energy integrals were found to be less consistent due to uncertainties in selecting a proper time window of integration.

Once the measurement geometry had been settled for each ping, the source level was determined using the calibrated hydrophones (no 8 and 14). It was obtained by adding the spreading loss along the direct path to the measured signal levels at these hydrophones. It was then noted that the source levels exhibited fluctuations up to 10 dB when the ship was drifting towards the array. On the receding path the source levels were found to be stable. Therefore only data on that portion of the track where the source was moving away from the receiver are used.

Averaging over the hydrophones and over a large number of pings from track 1 resulted in the following esimates [dB re 1 μPa] at 1 m:

$$500Hz : 163.7 \pm 0.4, \quad 1kHz : 162.6 \pm 1.1, \quad 2kHz : 161.0 \pm 1.3, \quad 4kHz : 156.0 \pm 0.7$$

The ping-to-ping variations at the same hydrophone was around 0.3 dB, while the difference between the hydrophones for frequencies larger than 500 Hz was of the order 1-2 dB.

Once the source level was established the sensitivity of the remaining 29 hydrophones were determined by comparisons of received and predicted signal levels for a large number of pings.

2.5 Acoustic data

A typical example of travel-time curves from the reflection loss measurements is shown in Fig. 2.6. The emitted pulse is the 4-kHz Ricker chirp $r_c[4, 15]$. The radial source-receiver distance is 65.0 m. The source depth is 15.5 m, which is also the depth of hydrophone 11. The trace of direct arrivals is smoothly curved because the distance to the source increases both upwards and downwards from hydrophone 11. The slope of the traces of reflected arrivals tells whether the last reflection took place at the sea surface or at the bottom. The identification of the traces in Fig. 2.6 as indicated by color labels was performed in two stages. First a time-window for the desired arrival was predicted using information about the source-receiver geometry, the bathymetry and the sound speed profile. After that the suggested time-window was searched for the peak value of the energy signal. If the level of the peak exceeded the background by 6 dB, the arrival of the peak was labeled. A few erroneous labels occur because of overlapping arrivals and faint amplitudes. The downward propagating wave, which arrives at 56 ms at the top hydrophone, is of unknown origin.

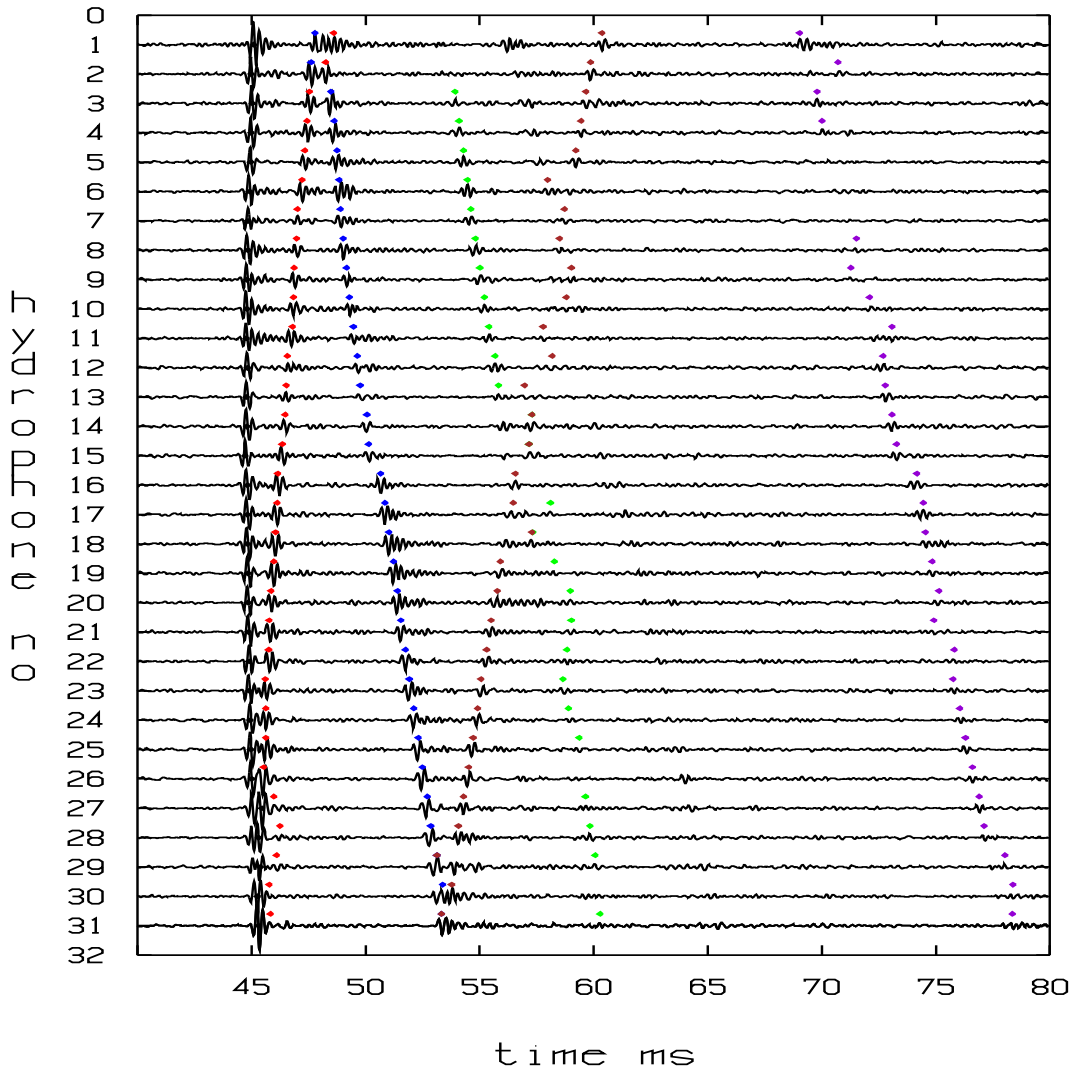

Figure 2.6: *Matched-filtered 4-kHz Ricker chirp travel-time curves at the array of receivers. The source-receiver range is 65.0 m. The arrivals form traces that are labeled as follows: sea surface reflected path (blue), the direct bottom bounce (red), the sea surface-bottom path (green), the bottom-sea surface path (brown), the sea surface-bottom-sea surface path (violet). The color labeling was based on identification of arrival times by searching for peak amplitudes in time-windows determined by the experimental configuration.*

There are four arrivals with exactly one bottom bounce. The inversions for the velocity of the bottom in Sec. 5 utilizes only the direct bottom bounce.

Fig. 2.7 (bottom panel) is an expanded portion of the signal in hydrophone 8. For comparison the corresponding 0.5, 1 and 2 kHz signals at the same hydrophone are shown. The signals are not aligned in time because the source is slowly moving away from the receiver during the transmissions. The bottom bounce is not discernable between the direct arrival and sea surface reflection at the 0.5 and 1 Khz signals.

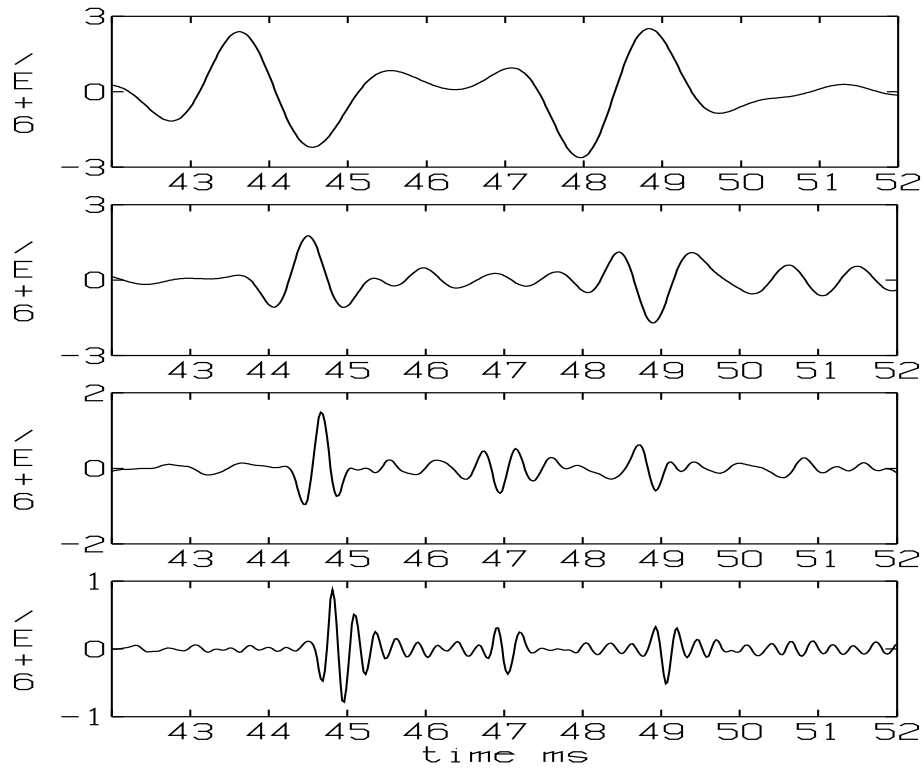

Figure 2.7: *Matched-filtered 0.5, 1, 2 and 4-kHz Ricker chirps (top to bottom)* $[\mu Pa]$ *at hydrophone 8 for a source-receiver range of some 65 m. The direct arrival, the bottom bounce and the sea surface reflection are well separated at 2 and 4 kHz.*

3 Determination of bathymetry

Figure 3.1 shows ray paths of the direct bottom bounces for the source-receiver separation 65.0 m, that is the same configuration as in Fig. 2.6. A few hydrophones at the top and bottom of the array have been exluded, because of overlapping arrival times, see Fig. 2.6.

The ray diagram was drawn under the assumption that the water depth is constant over the source-receiver range. When the traveling times along these rays are computed and compared with the measured ones, it is found that the average difference is 0.43 ms, which is larger than the expected time accuracy 0.3 ms. To correct for the difference, the water depth $h(r)$ is assumed to vary linearly by range according to

$$h(r) = h_0 + r \cdot \tan\alpha \tag{3.1}$$

where h_0 is the water depth at the receiver array (27 m) and r is the range coordinate. For each hydrophone a value of the angle α was determined by equating the measured and calculated travel times. The latter one was obtained by ray tracing for the sloping bottom (3.1). When the optimal angle had been determined, the water depth at the reflection point at the sloping bottom is obtained by inserting the distance to the reflection point into (3.1). The estimates of the water depth is limited to the ranges of the reflection points, which in the present case extends from 15 to 41 m. The resulting bottom profile is shown in Fig. 3.2. The variation of the water depth corresponds to a

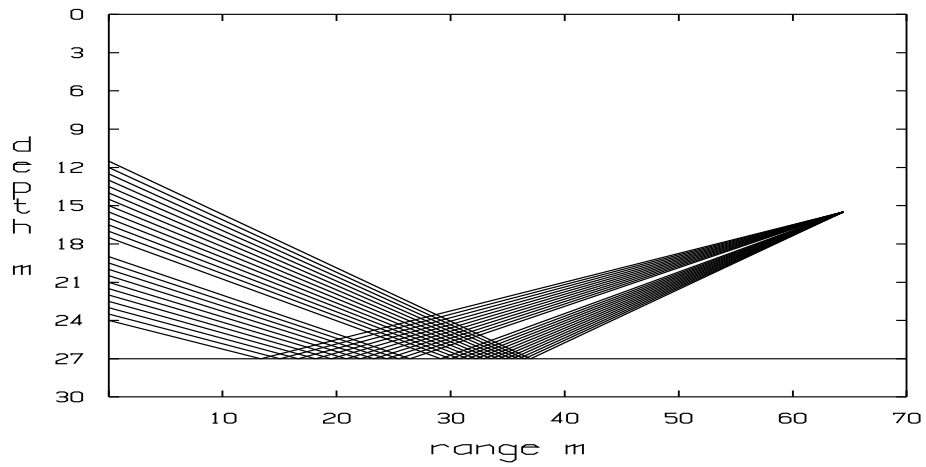

Figure 3.1: *Ray diagram of direct bottom paths for a flat bottom.*

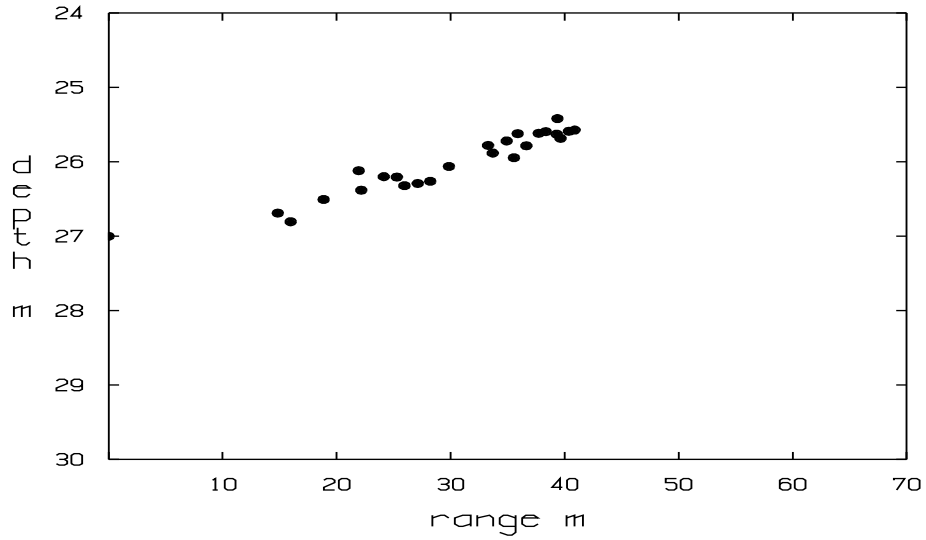

Figure 3.2: *Estimated water depths using arrival times of bottom bounces for a source-receiver range of 65.0 m.*

bottom slope of 3°. The results of the inversion for bathymetry using all 4-kHz pings along track 1 are shown in Fig. 3.3.

It should be noted that the directions of the straight line connections between the moving source and the receiver array vary along the track, which implies that the estimates of the water depth cover a portion of the area swept out by these lines. This is precisely the patch of the seafloor which is targeted by the inversion scheme in Sec. 5.

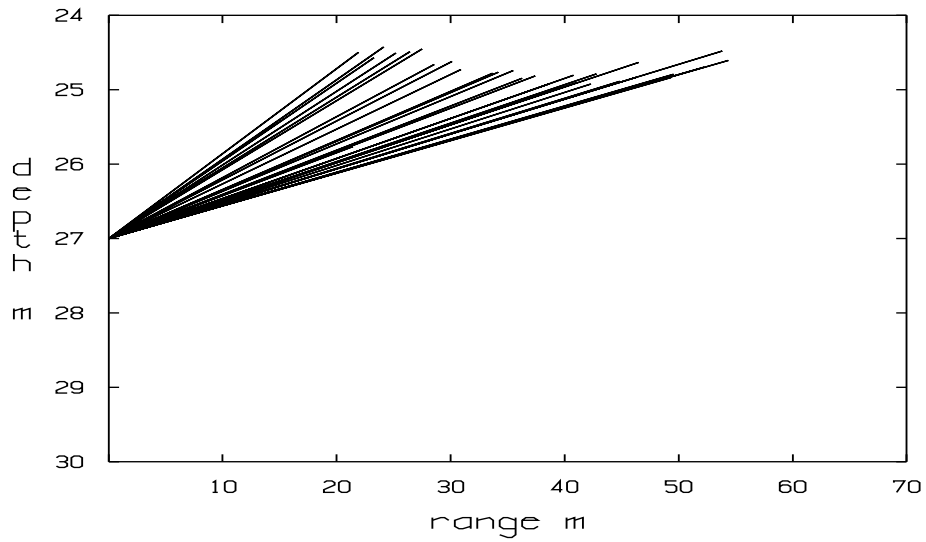

Figure 3.3: *Estimated bathymetry using bottom bounces along track 1. The slopes form a fan because the track is not entirely radial from the receiver position.*

4 Wave height estimation

At wind speeds around 10 m/s sea surface scattering of acoustic waves in mid-frequency bands is appreciable [6]. A measure of the scattering effect is given by the coherent surface reflection coefficient [7],[8].

$$R_c = -e^{-\frac{P^2}{2}} \tag{4.1}$$

where P is the Rayleigh parameter

$P =$ $2k\sigma \sin\theta$,

$k =$ $\frac{2\pi}{\lambda} = \frac{2\pi f}{c}$, wavenumber $[m^{-1}]$,

$c =$ speed of sound $[m/s]$,

$f =$ frequency $[Hz]$,

$\theta =$ grazing angle,

$\sigma =$ rms wave height, $[m]$.

It implies that the reflection loss $-20log|R_c|$ can be written as

$$R_{loss} = 685.8(\frac{\sigma \sin\theta}{\lambda})^2 \quad [dB]. \tag{4.2}$$

The correlation between wind speed and wave height depends on the duration of the wind and local hydrographic conditions. There are several approximate formulas for the rms wave height as function of wind speed, one of which is given by

$$\sigma = 0.0053v^2, \quad [m], \quad v = \text{wind speed}, \quad [m/s]. \tag{4.3}$$

The formula (4.3) can be derived theoretically using the Pierson-Moskowitz surface wave spectrum for a full developed sea [9]. Table 4.1 shows evaluations of the reflection

loss (4.2) for $v = 10$ m/s, or $\sigma = 0.53$ m, and for $\theta = 2°$ and $\theta = 20°$, which are typical grazing angles of surface reflections at source-receiver separations of 1 km and 100 m respectively.

$\theta[deg]$	frequency $[kHz]$			
	0.5	1	2	4
2	0.03	0.1	0.45	1.8
20	2.6	10.7	43	171

Table 4.1: *Surface reflection loss according to formula (4.2) as function of grazing angle and frequency. The rms wave height is 0.53 m.*

Apart from excessively large losses, which just imply that the coherence is lost, the figures indicate that scattering loss at the sea surface is an issue at mid-frequencies. Since wave height is a more significant parameter than wind speed in this context, it is of interest to estimate the wave height by inversion of reflection data. Fig. 4.1 shows time-windowed amplitudes of sea surface reflections received at hydrophones 11-20 for a source-receiver separation of 65.0 m. The amplitude at each hydrophone is

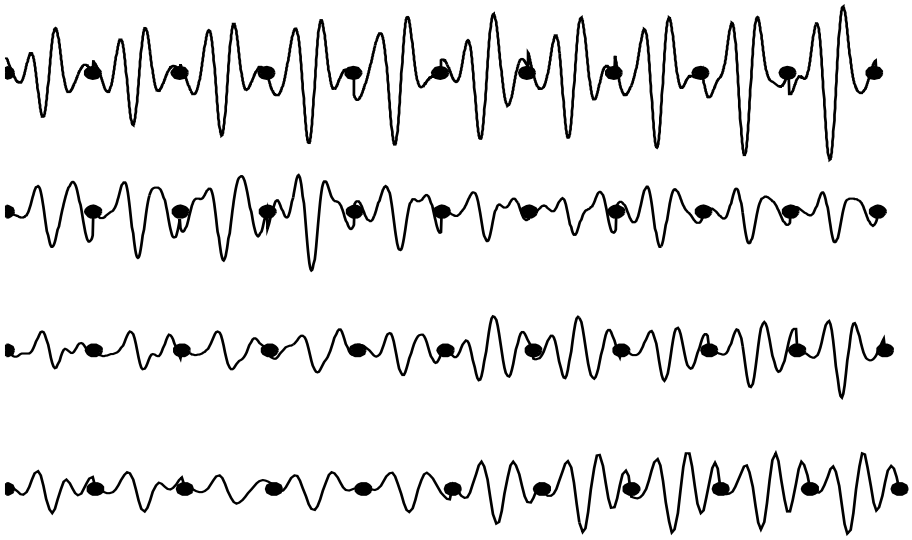

Figure 4.1: *Time-windowed waveforms of sea surface reflections received at hydrophones 11-20 for 0.5, 1, 2 and 4 kHz (top to bottom) for a source-receiver separation of 65.0 m. The time scale of the rows 2, 3 and 4 has been expanded by a factor 2, 4 and 8 respectively relative to the top row.*

normalized by the peak value of the direct arrival at the same hydrophone. Therefore information of the reflection coefficient is displayed by comparing amplitudes in Fig. 4.1. As predicted by the theoretical formula (4.1), the amplitudes diminish at increasing frequencies. The average reflection losses for the signals shown in Fig. 4.1 were 0.17, 3.5, 6.3 and 6.6 dB in the order of increasing frequencies.

In fitting the model (4.1) to measured values of R_c, the range of usable P-values is restricted by two considerations. If P is too large, the coherence is too small and incoherent scattering would dominate. As an upper bound for P, we shall apply the

well-known Rayleigh criterion $P < \pi/2$ for the borderline between a smooth and a rough surface as it appears when viewed from a given angle with a signal of a given frequency. If P is too small, the loss is less than the measurement error. To avoid this situation a reasonable lower bound is $P > 0.5$, which corresponds to a reflection loss of 1 dB. Therefore angles and frequencies useful for inversion of wave height should be within the range

$$0.5 < P < \frac{\pi}{2}. \tag{4.4}$$

The criterion (4.4) involves the rms wave height, which is unknown prior to the inversion. Here a tentative value of the wave height from the wind speed formula (4.3) can be inserted when data for inversion are screened with respect to the criterion (4.4). This approach was applied to 4-kHz data for grazing angles in the range 15° to 30°. The fitness function was formulated as the rms difference of the measured and modeled losses with the wave height as the single target parameter. Due to the large statistical variability of measured values, averaging over angular intervals of 5° was applied. The inversion resulted into a wave height of 6 cm. The goodness of the best fit was 1 dB. Figure 4.2 shows averaged reflection loss and loss curves from the model (4.2) for the wave heights 4, 6 and 8 cm.

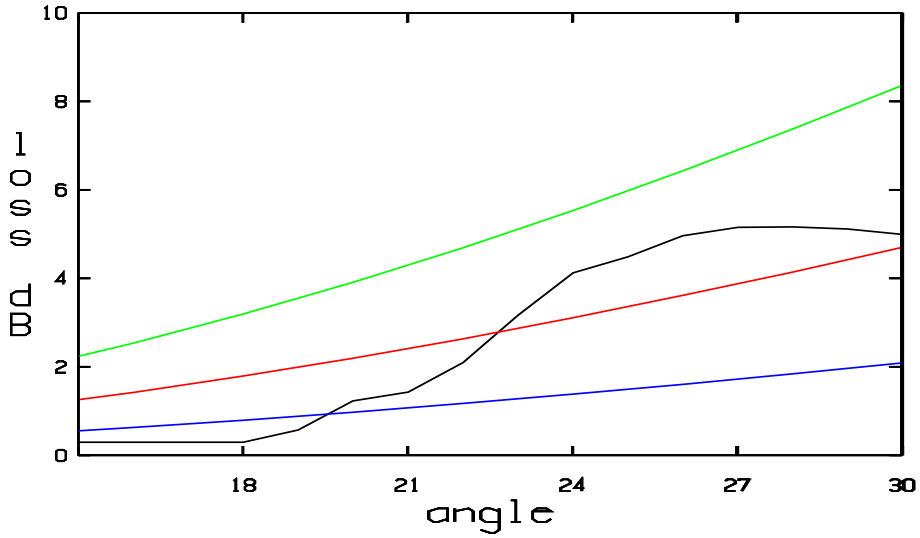

Figure 4.2: *Averages of measured (black) reflection loss at 4 kHz versus grazing angle and correspondingly for the model (4.2) with the wave height set to 4 (blue), 6 (red) and 8 (green) cm.*

5 Geoacoustic inversion

5.1 Modeling considerations

A geoacoustic model is a description of the acoustic bottom parameters and their distribution in range and depth. It is part of the input to the wave propagation model along with information of bathymetry and source excitation. In this study a two-layer bottom model was adopted for inversion. The top layer is assumed to be very thin and

soft with fluid-like properties. The underlying sediment layer is assumed to be hard and it constitutes the main reflector. This layer is allowed to support shear waves, if applicable. It can be considered as semi-infinite in view of the poor penetration depth (10 m or less) of the signals being used. This is a typical model for sandy sediments. Observations of grab samples frequently show that the upper few tens of centimeters of the sediment column has a velocity which is somewhat less than that of the water at the bottom [10], [11], [12]. When the thickness of this layer is less than a wavelength, its acoustic impact is mostly insignificant when the underlying substrate is hard. However notable exceptions occur when the thickness is of the order a quarter of a wavelength. Then the layer may act as a coupler between the seawater and the basement and high reflection losses may occur even at small grazing angles [13]. In shallow water this layer may be highly variable both in depth and range depending on varying depositional processes.

Conversion to shear waves, which are absorbed or escape to greater depths, is a loss factor which increases by the shear velocity. Although the effect is larger at low frequencies, the loss is appreciable at a few kHz for shear velocities larger than 400 m/s [14]. For fine grained sandy sediments the shear velocity is less than that, and the shear effects can be neglected. As this simplifies the modeling, the case without shear rigidity should not be ignored in the progress towards more complex geoacoustic models. Counting the special cases without a soft covering and no shear rigidity as independent models, we end up with four trial models. They are denoted by FF, FS, FFF and FFS, where F=fluid, S=solid is the type of layer in a stratigraphy including the water layer. Figure 5.1 illustrates typical behaviour of the reflection loss for plane waves (Rayleigh reflection) at 4 kHz and for the parameter set (sound velocity, density, absorption)

$$\begin{aligned} \text{water layer:} \quad & c_1 = 1435, \quad \rho_1 = 1.0, \quad \alpha_1 = 0.0 \\ \text{soft sediment:} \quad & c_2 = 1400, \quad \rho_2 = 1.3, \quad \alpha_2 = 0.1 \\ & d = 0.4 \quad [m], \quad \text{(thickness)} \\ \text{hard sediment:} \quad & c_3 = 1700, \quad \rho_3 = 1.8, \quad \alpha_3 = 0.3 \\ & c_s = 400, \quad \alpha_s = 0.5 \end{aligned} \tag{5.1}$$

with the units $[m/s, g/cm^3, dB/\lambda]$. The FF, FS and FFF models are obtained by setting $d = 0$ and/or $c_s = 0$.

A distinctive feature of all models is that high losses sets in as grazing angles exceeds the critical angle θ_c

$$\theta_c = \cos^{-1} \frac{c_1}{c_3} = \cos^{-1} \frac{1435}{1700} \approx 32^\circ.$$

In the FF case and no sediment absorption ($\alpha_3 = 0$) the reflections would be lossless at angles less than θ_c. This is not the case when the sediment has some rigidity as energy is carried away to greater depths by shear waves. The shear effect is weak at $c_s = 400\ m/s$ as can be seen from Fig. 5.1, but it increases rapidly at larger shear speeds. The impact of a sediment cover of mud type can be seen by the loss curves of the models FFF (green) and FFS (red). The thickness of the top sediment is merely 0.4 m or around one wavelength at 4 kHz. There are two local loss maxima, one at 4° and the other one at 43°. By trial computations it was found that the peak at

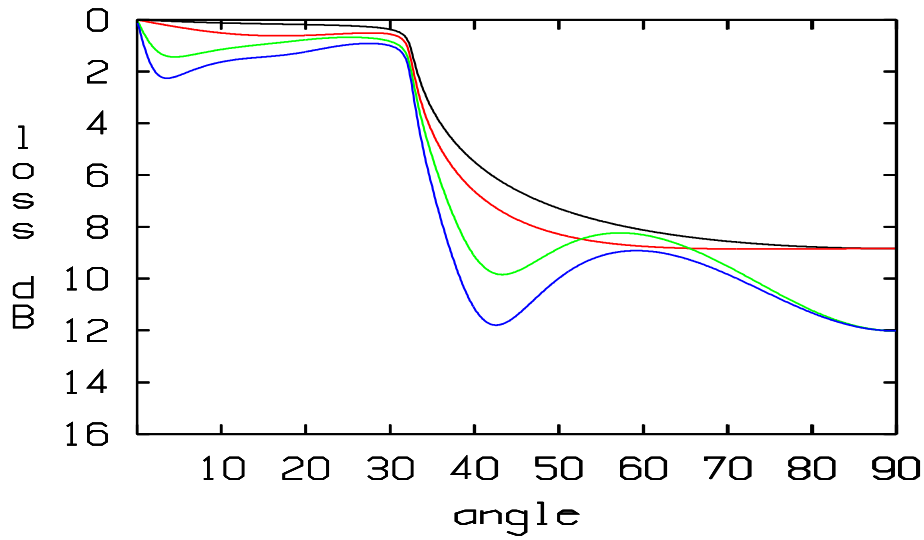

Figure 5.1: *Reflection loss versus grazing angles for the models FF (black), FS (red), FFF (green) and FFS (blue) for 4 kHz and the geoacoustic parameters 5.1.*

4° disappears when the absorption of the soft layer is set to zero ($\alpha_2 = 0$). The loss maximum at the steeper angle 43° is caused by an impedance match of the water layer and the hard sediment by the intermediate layer. This feature is sensitive to the wavelength/thickness ratio as can be observed from Fig. 5.2.

The basic assumption behind Rayleigh reflection is that the media interfaces, as well as the wavefronts of the sound waves, are plane. The discrepancy between spherical and plane wave reflections at a plane boundary between two semi-infinite homogeneous media is analyzed in [7]. The analysis shows that the Rayleigh model is accurate provided that the source/receiver positions are not too close to the interface relative to the wavelength, and secondly, the angle of incidence must not be too close to the critical angle. The deviations are inversely proportional to the frequency. In order to check the accuracy of the Rayleigh model, a full-field model for a point source emitting spherical waves has been used in this study. Figure 5.2 shows comparisons between spherical and plane wave reflections computed at an array of receivers located 1 m above the seafloor at distances ranging from 0.2 to 1432 m for which the grazing angles at bottom reflections run from 89° to 0.5°. As predicted by theory, departures occur mostly around the critical angle and they decrease at higher frequencies. On the large, the Rayleigh model is surprisingly good in view of its simplicity. The 7-dB difference between 1 and 2 kHz at normal incidence, which is common for the two models, is notable. The larger loss at 1 kHz is explained by the fact that the thickness of the intermediate layer is around one quarter of a wavelength.

In the experiment reflection loss data are extracted from the measured time series using the peak amplitude of the envelope squared of matched filtered Ricker chirps in a time-window centered at the arrival time of the bottom echo. The bandwidth of signals are $\approx 0.8 f_c$, where the center frequencies f_c= 0.5, 1, 2 and 4 kHz were used. Figure 5.3 shows bottom echoes as computed by FFT-synthesis using both the full-field (black) and the Rayleigh (red) model. The center frequency is 500 Hz and the grazing angle

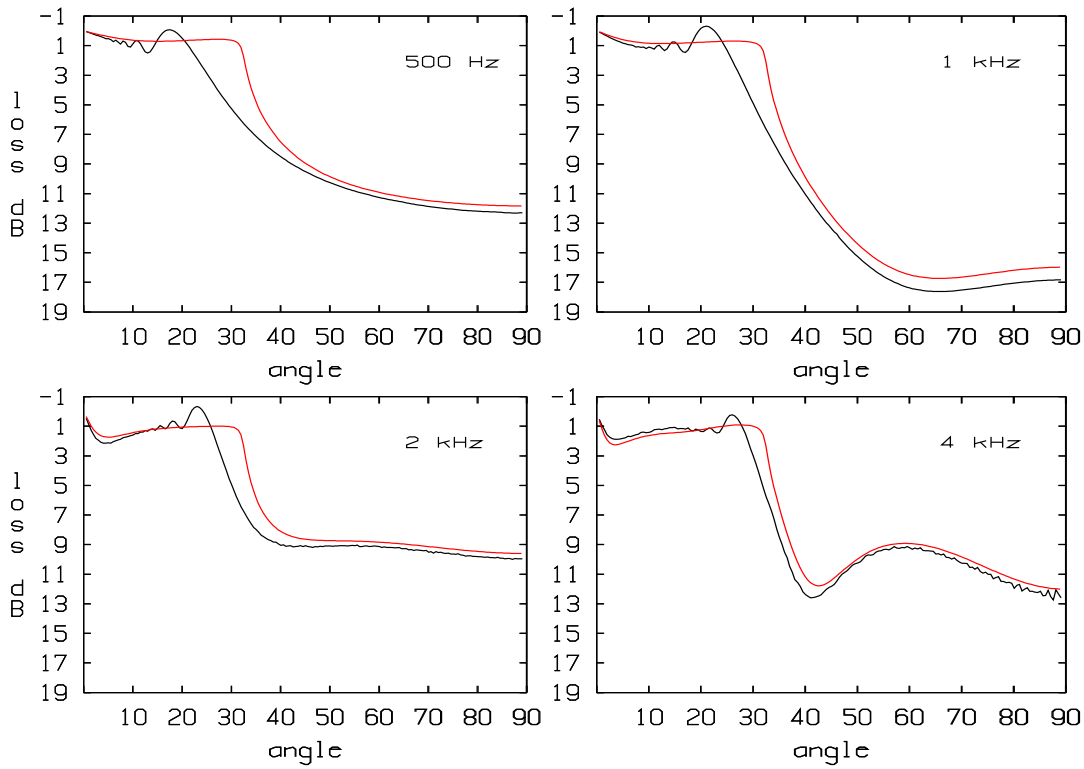

Figure 5.2: *Reflection loss versus grazing angle for spherical (black) and plane (red) wave reflections at 0.5, 1, 2, and 4 kHz for the three-layer model FFS with the bottom parameters 5.1. The source of the spherical waves is a monopole with the height 11.5 m above the seafloor. Reflection loss is obtained at receivers 1 m above the seafloor at ranges from 0.2 to 1432 m.*

is close to the critical one. In this case it can be seen from Fig. 5.2 that the Rayleigh model underestimates the reflection loss by some 5 dB. Loss calculations based on the peak amplitudes of the pressure curves displayed in Fig. 5.3 show good agreement ($<$ 0.1dB) with those for cw-signals at the center frequency 500 Hz. In comparing reflection loss of frequency and time domain solutions, it should be noted that the reflection coefficient of the cw-model represents the compound response of a layered structure, while pulse propagation gives rise to a sequence of echoes as layer interfaces are encountered. In the present study there is no significant difference between these approaches as the reflectivity of surficial sediment is relatively small and its thickness is commensurate with the wavelength. For a bottom of silty-clay type the soft layer is larger, which leads to time-separated echoes from the interfaces of the FFF and FFS models. Inversion techniques for such low-velocity sediments are considered in [15], [5], [16].

5.2 The inversion scheme

The inversion for bottom parameters is based on matching of measured and computed reflection loss for a suite of source-receiver geometries. A best fit is obtained by mini-

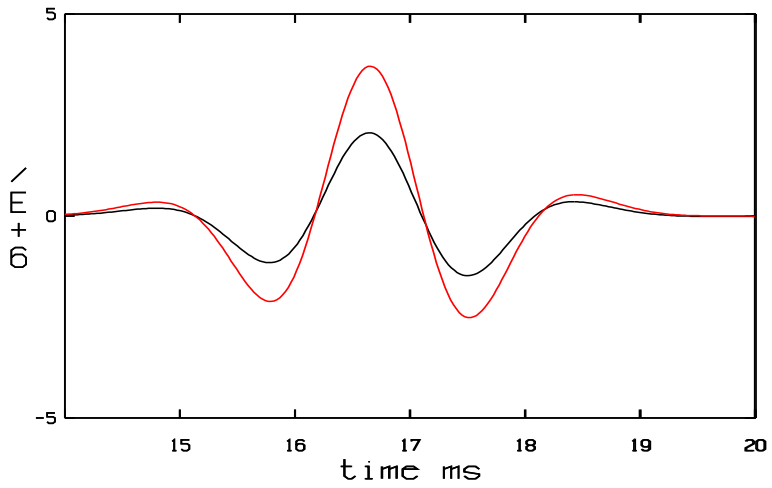

Figure 5.3: *Time domain solutions* $[\mu Pa]$ *of the bottom echo computed by the full-field (black) and the Rayleigh (red) models for the bottom parameters 5.1. The transmitted signal is a Ricker pulse centered at 500 Hz for a source level of 160 dB. The source and the receiver heights above the seafloor are 11.5 and 1 m respectively and their horizontal separation is 20 m corresponding to a grazing angle of* 32° *at the bottom reflection.*

mizing the fitness (or cost) function

$$F[s] = \left(\frac{1}{M} \sum_{m=1}^{M} (R_m^{dat} - R_m^{mod}[s])^2 \right)^{\frac{1}{2}}, \quad [dB] \tag{5.2}$$

where

$$\begin{aligned} \text{M} &= \text{number of observations} \\ R_m^{dat} &= \text{measured reflection loss} \\ R_m^{mod}[s] &= \text{computed reflection loss} \end{aligned}$$

Here $s \in S$ represents a specific set of bottom parameters drawn from the search space S, which in this study is spanned by 3 to 9 parameters depending on the choice of geoacoustic model. These parameters are input to the propagation model, which delivers synthetic loss values $R_m^{mod}[s]$. In principle one inversion is applied for each combination of geoacoustic model, propagation model and data. The present data comprises reflection loss measurements from transmissions of four different pulses along four tracks. Only a selection of inversions are presented below.

The high dimension of the search space, which typically has many local minima of the cost function, makes it necessary to use a global search method. The inversions in this paper use a genetic algorithm (GA), which is based on genetic biological principles [17]. Software for matched-field inversion includes program blocks for geoacoustic models, wave propagation, cost function definitions and search algorithms. A number of independent choices can be made for each component. In order to make it easier to compile an inversion package from a number of off-the-shelf modules, a general software is under development.

5.3 Inversion results

The search bounds and the discretization steps for the parameterization of the geoacoustic models are shown in Table 5.1.

search	soft sediment				hard sediment				
bounds	d	c_2	ρ_2	α_2	c_3	ρ_3	α_3	c_s	α_s
initial value	0.01	1380	1200	0.07	1400	1400	0.1	100	0.1
final value	0.5	1420	1500	0.2	1900	1600	0.5	600	2.0
step size	0.03	2.7	20	0.01	8	13	0.03	16	0.06

Table 5.1: *The discrete search space of target parameters.*

The key parameter of the inversion is the sound velocity of the hard sediment. Its bounds are set wide, while those for the density and absorption are tightly constrained. The reason is that unphysical parameter sets with large densities, high absorption and low velocities occasionally turn out to be optimal. It would thereby obscure a realistic solution whose fitness could be satisfactory relative to measurement and modeling uncertainties. A common way to alleviate the ambiguity is to exclude the density from the search space and instead couple the density to the velocity by an empirically derived regression formula [4], [18]. However, this approach precludes an accurate determination of the density which is possible in specific cases. For example, inversions for the density using reflection loss data both at normal and oblique incidence, or exploiting the angle of intromission of low-velocity sediments, are well conditioned [15].

5.3.1 Track 1, 500 Hz

The number of bottom echoes that can be safely isolated from the direct and the surface reflected waves increases by the frequency and by the proximity of the closest point of approach (CPA). Due to the poor resolution of the 500 Hz pulse, and with a CPA of 34 m at track 1, only a small set of reflection loss observations (68) was available for inversion in this case. Figure 5.4 displays measured data and the inverted loss curve for the FF model. The inversion results are listed in Tab. 5.2.

geo-	fitness	soft sediment				hard sediment				
model	dB	d	c_2	ρ_2	α_2	c_3	ρ_3	α_3	c_s	α_s
FF	1.8	—	—	—	—	1551	1600	0.50	—	—
FS	1.8	—	—	—	—	1551	1600	0.50	100	2.0
FFF	1.8	0.01	1404	1200	0.12	1551	1600	0.50	—	—
FFS	1.8	0.03	1420	1500	0.07	1551	1600	0.50	100	2.0

Table 5.2: *Inversion results for track 1, 500 Hz and for the Rayleigh model.*

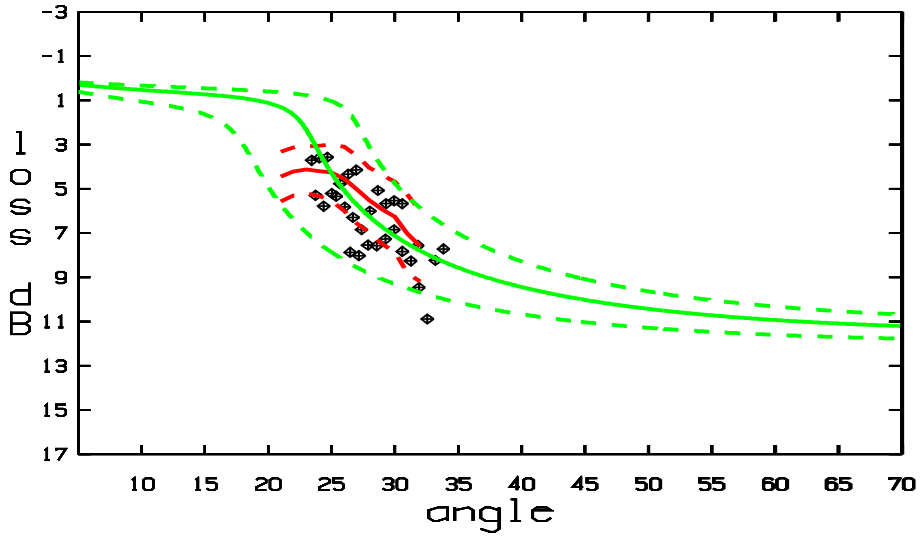

Figure 5.4: *Track1, 500 Hz: Reflection loss data (black), angular averages (red solid),standard deviations (red dashed) and the best fit loss curve (green) for the FF model. Dashed green curves are loss curves for sediment velocities* ± 50 *m/s from the optimal one.*

The velocity is the only parameter that is well-determined by data. Although the angular interval of reflection loss data is narrow, it comprises part of the angular domain just beyond the critical angle. This area is sensitive to changes of the velocity regardless the choice of model. We also see that the inversion results are unambiguous.

5.3.2 Track 1, 4 kHz

At 4 kHz the number of reflection loss observations amounts to 509. This data set was divided into two groups, one for which the horizontal distance between the receiver array and the target points of the bottom bounces at the seafloor was less than 25 m (proximal area), and the other one for hit points beyond 25 m (distant area). These groups are related to the horizontal source-receiver offset, but they do not coincide, because the vertical extent of the receivers implies that both the location and angle of the bottom bounces vary. As displayed in Figs. 5.5 and 5.6 both the loss and the variability is larger at the distant area. The inversion results are listed in Tab. 5.3 and 5.4.

geo-	fitness	soft sediment				hard sediment				
model	dB	d	c_2	ρ_2	α_2	c_3	ρ_3	α_3	c_s	α_s
FF	1.7	—	—	—	—	1622	1600	0.50	—	—
FS	1.4	—	—	—	—	1717	1400	0.50	552	2.0
FFF	1.3	0.24	1420	1500	0.20	1694	1600	0.50	—	—
FFS	1.3	0.24	1420	1500	0.07	1757	1400	0.50	600	1.8

Table 5.3: *Inversion results for track 1, 4 kHz, proximal area and for the Rayleigh model.*

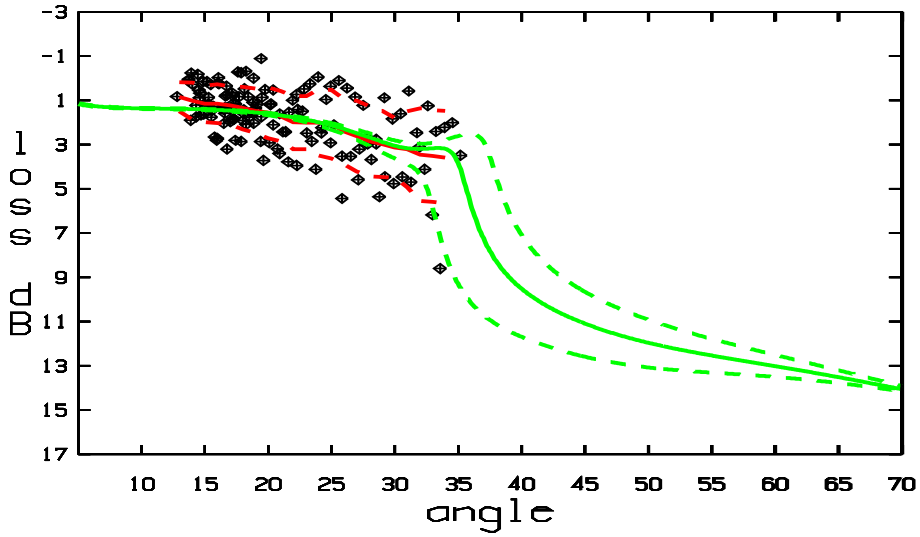

Figure 5.5: *Track 1, 4 kHz, proximal area: Reflection loss data (black), angular averages (red solid), standard deviations (red dashed) and the loss curve of best fit (green) for the FFS model. Dashed green curves are loss curves for sediment velocities* ± 50 *m/s from the optimal one.*

geo-	fitness	soft sediment				hard sediment				
model	dB	d	c_2	ρ_2	α_2	c_3	ρ_3	α_3	c_s	α_s
FF	3.4	—	—	—	—	1479	1600	0.50	—	—
FS	3.5	—	—	—	—	1487	1600	0.50	100	2.0
FFF	2.8	0.40	1420	1500	0.20	1519	1600	0.50	—	—
FFS	2.8	0.37	1420	1360	0.20	1575	1600	0.50	600	2.0

Table 5.4: *Inversion results for track 1, 4 kHz, distant area and for the Rayleigh model.*

Data indicate that the sediment becomes softer and more heterogenous at larger distances from the array. The predicted velocity of the proximal area is in the range 1620-1750 m/s, which exceeds the velocity predictions of the distant area by some 100 m/s. The change takes place within a distance of 50 m. Data for the 500 Hz inversion in Sec. 5.3.1 comprises bottom bounces evenly spaced in ranges 20-33 m, which appears to be the transition zone from harder to softer sediments. The inversion results for the 500 Hz case is also intermediate to those above.

As a consistency check fitness values for the optimal parameter sets were evaluated for reflection loss data at 2 kHz. For the optimal FFS model of the proximal area the fitness of 2 kHz data were found to be 2.0 dB. This is slightly worse than the best fit of 1.3 dB for the 4 kHz case. A visual inspection of the data sets show that they are similar. Data for 2 and 4 kHz at the distant area are also similar. However, when the FFF parameters from the inversion were tried on 2 kHz data , the fitness dropped from 2.8 to 8.6 dB. The reason is that the loss sink seen at 40° for the best fit in Fig. 5.6 moves to 25° for a change of frequency from 4 to 2 kHz, which results in a large misfit with data. This example illustrates the difficulties of obtaining consistent estimates with the thin layer model for different frequencies. Turning to the optimal FF model

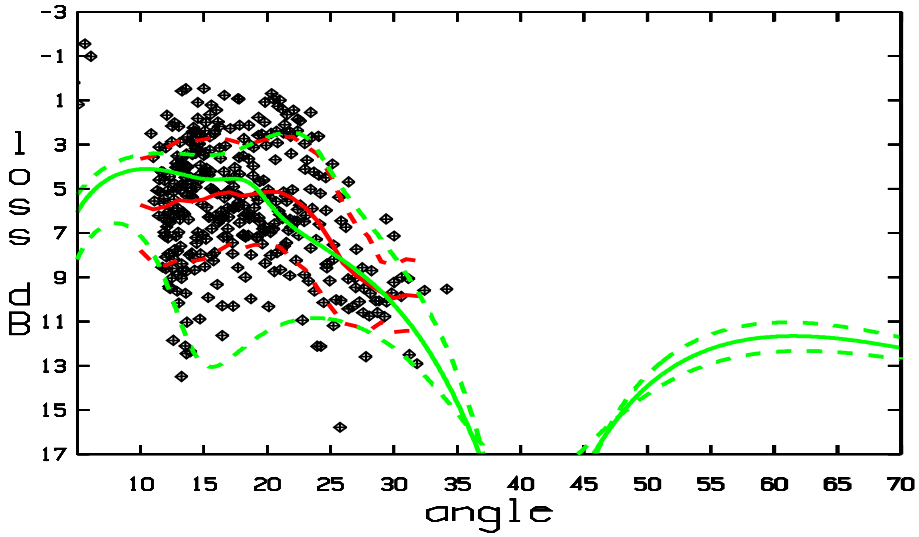

Figure 5.6: *Track 1, 4 kHz, distant area: Reflection loss data (black), angular averages (red solid), standard deviations (red dashed) and the loss curve of best fit (green) for the FFF model. Dashed green curves are loss curves for sediment velocities* ± 50 *m/s from the optimal one.*

instead, when it is applied to track 1, 2 kHz, distant area data, the fitness worsens from the optimal 3.4 dB at 4 kHz to 4.5 dB. This drop is acceptable in view of the uncertainties of data.

5.3.3 Track 3, 0.5 and 4 kHz

The CPA of track 3 was merely 15 m, which resulted in reflection loss data at larger grazing angles than elsewhere. The nearness also increases the time separation between the different arrivals, which made it possible to extract many observations (348) at 500 Hz. However those data were limited to grazing angles larger than 27° because of insufficient time separation of bottom bounces at more shallow angles. However the angular domain can be extended to smaller angles by using the shorter 4 kHz-pulses. Therefore an inversion for track 3 was performed on 500 Hz data supplemented with a subset of 4 kHz data at low grazing angles. The total number of observations was 763. Figure 5.7 displays the combined data set and the inverted loss curve for the FF model. The inversion results are listed in Tab. 5.5.

geo-	fitness	soft sediment				hard sediment				
model	dB	d	c_2	ρ_2	α_2	c_3	ρ_3	α_3	c_s	α_s
FF	2.4	—	—	—	—	1511	1600	0.50	—	—
FS	2.4	—	—	—	—	1511	1600	0.50	100	2.0
FFF	2.4	0.01	1380	1200	0.07	1511	1600	0.50	—	—
FFS	2.4	0.01	1380	1200	0.07	1511	1600	0.50	100	2.0

Table 5.5: *Inversion results for track 3, using both 0.5 and 4 kHz and for the Rayleigh model.*

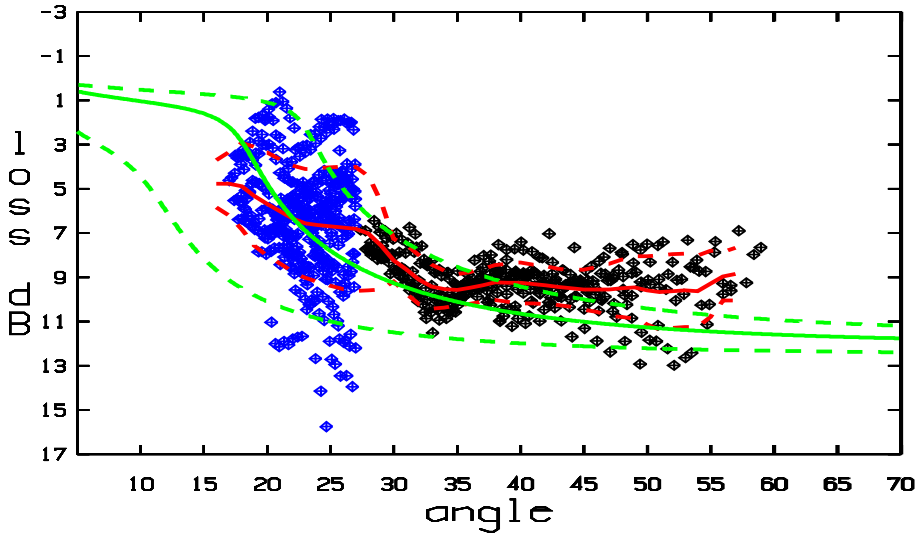

Figure 5.7: *Track 3, 0.5 and 4 kHz: Reflection loss data 500 Hz (black) and 4 kHz (blue), angular averages (red solid), standard deviations (red dashed) and the loss curve of best fit (green) for the FF model. Dashed green curves are loss curves for sediment velocities* ± 50 *m/s from the optimal one.*

The standard deviation around the mean value at each grazing angle is a measure of the variabiltity of data. The relatively larger spread at 4 kKz as can be observed in 5.7 is a typical feature. A presumable explanation is that bottom scattering increases by the frequency. The inversion results of all models agree very well.

5.3.4 Track 4, 4 kHz

Reflection loss data at track 4 were confined to the last third of the track because the source level could not be ensured until the ship had passed the receiver array, see Fig. 2.3. At the end of the track, track 1 is intersected at an area where the velocity was found to be lower than elsewhere according to the inversion results for track 1. Therefore reflection loss data at track 4 was divided into two groups with respect to source positions relative to track 1. Pings emitted in an area located farther away than 50 m from track 1 were placed in the first group, while the second group comprises loss data from source positions within 50 m from track 1. Figure 5.8 shows reflection loss data of the first group in black dots and those from the second group in blue. The inverted loss curve for group one is shown by a green solid line. The inversion results for group one data are listed in Tab. 5.6. The inversion results are based on 483 observations.

The disparity of reflection loss between the two parts of track 4 is obvious from the black and blue data sets in Fig. 5.8. Although the velocity estimate around 1620 m/s is unambiguous for all models, a larger velocity is conceivable as suggested by the dashed curve for 1670 m/s in Fig. 5.8. Lack of data for larger grazing angles precludes a more definite estimate.

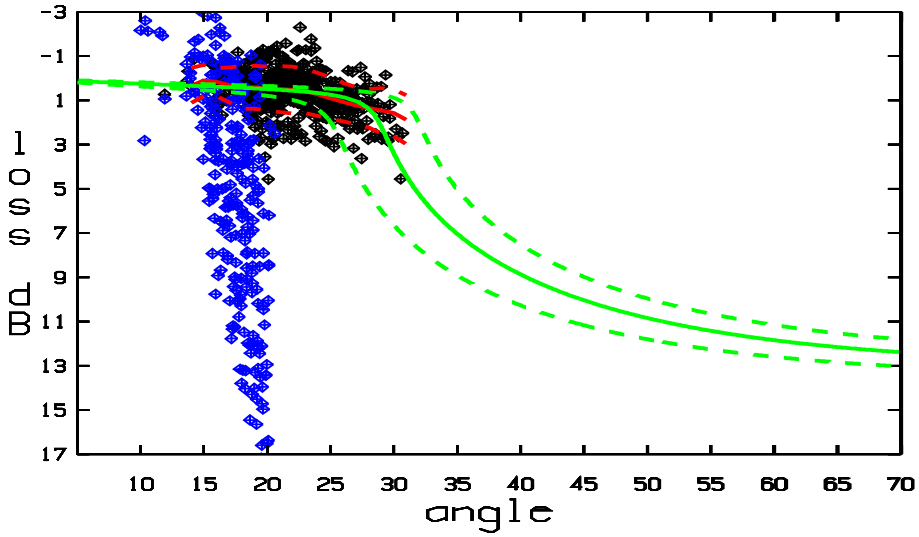

Figure 5.8: *Track 4, 4 kHz, area 50 m beyond track 1: Reflection loss data (black), angular averages (red solid), standard deviations (red dashed) and the loss curve of best fit (green) for the FF model. Dashed green curves are loss curves for sediment velocities ±50 m/s from the optimal one. Reflection loss data from source positions within 50 m from track 1 are labeled in blue.*

geo-model	fitness dB	soft sediment				hard sediment				
		d	c_2	ρ_2	α_2	c_3	ρ_3	α_3	c_s	α_s
FF	1.0	—	—	—	—	1622	1400	0.50	—	—
FS	1.0	—	—	—	—	1622	1400	0.50	116	0.10
FFF	1.0	0.01	1420	1200	0.10	1622	1400	0.50	—	—
FFS	1.0	0.01	1420	1500	0.08	1614	1600	0.50	100	0.16

Table 5.6: *Inversion results for track 4, 4 kHz, area 50 m away from track 1, and for the Rayleigh model.*

5.4 Inversion assessments

The only parameter of significance for the fitness is the velocity of the hard sediment. The impact of this parameter is made clear by the dashed green lines in Figs. 5.4-5.8, which are reflection loss curves for a ±50 m/s change of velocity of the best fit. A common way to gain information about the significance of an inversion parameter is to plot all cost function values with respect to the corresponding parameter visited during the GA search. Figure 5.9 show scatter plots of fitness values for the velocity and the density for the track 3, 0.5 and 4 kHz, model FFF inversion using a broadband plane wave propagation model.

The sensitivity of the sound velocity is made evident by the presence of a unique minimum around 1511 m/s, and the clustering of points around the optimal value. For the density there is a hardly noticeable tendency for larger values.

The accuracy of the single-frequency Rayleigh model was controlled by broadband propagation models based on FFT synthesis of both spherical (full-field) and plane

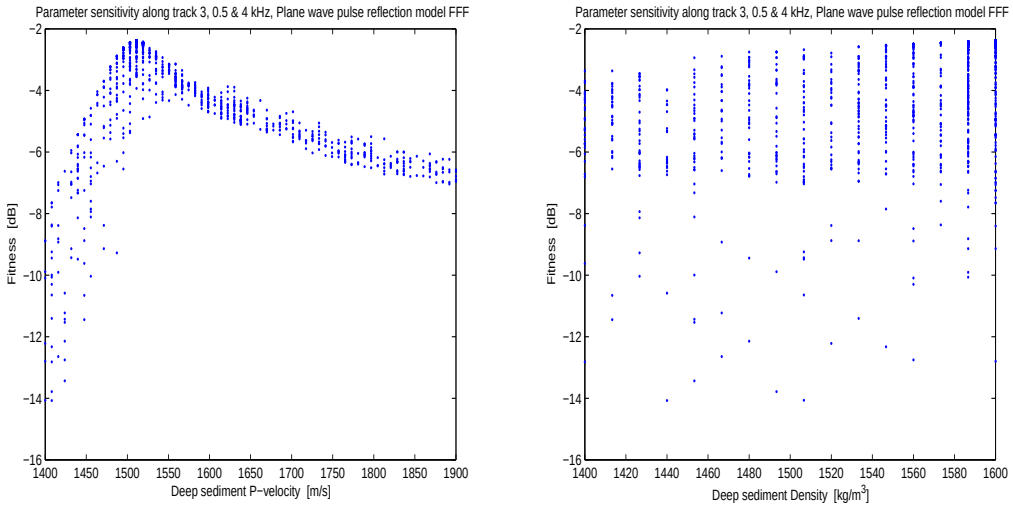

Figure 5.9: *Scatter plots of cost function values during the broadband GA inversion of track 3, 0.5 and 4 kHz data using the FFF model with respect to the the sound velocity (left) and the density (right) of the hard sediment.*

wave reflections. The case of bottoms with a constant slope is trivially accomodated in models for the direct bottom bounce, because the sea surface need not to be taken into account. The run time for a single evaluation of reflection loss by a broadband model is 0.04 and 0.5 seconds when the synthesis is based on plane wave and spherical reflections respectively. In comparison such an evaluation takes $2\mu s$ by the single-frequency Rayleigh model. Therefore broadband inversions were applied only in a few selected cases for a cross-check of the inversions made by the Rayleigh model. When the full-field model was run with the optimal parameter sets from the track 3 inversions the fitness value 2.3 dB was obtained for all models. This is slightly better than that for the Rayleigh model (2.4 dB), although no inversions were made. The run time for single evaluation of the fitness function on track 3 data takes is 10 minutes, which is too slow to be useful for inversion. However reasonable run times with a broadband propagation model is achieved when the Rayleigh model is used to compute the reflections at each frequency component of the emitted pulse. The inversion results of track 3 data using broadband modeling with plane wave reflections are shown in Tab. 5.7.

geo-model	fitness dB	soft sediment				hard sediment				
		d	c_2	ρ_2	α_2	c_3	ρ_3	α_3	c_s	α_s
FF	2.4	—	—	—	—	1511	1600	0.5	—	—
FS	2.4	—	—	—	—	1511	1600	0.5	100	1.33
FFF	2.4	0.01	1380	1200	0.07	1511	1600	0.5	—	—
FFS	2.5	0.08	1399	1200	0.19	1511	1600	0.5	100	1.88

Table 5.7: *Inversion results for track 3, 0.5 and 4 kHz, and for the broadband model with plane wave reflections.*

The good agreement between the inversion results in Tab. 5.5 and 5.7 assures the use of the Rayleigh model for these inversions. The reason for this is that reflection loss of

the FF and FS models are independent of the frequency. The optimal FFF and FFS models are also independent of the frequency in this case, because the thickness of the thin layer is neglibly small. In general, the FFF and FFS models should be applied with some caution at single frequency inversions of broadband signals due to frequency effects related to the thickness of the intermediate layer.

On the whole the inversion results of all models are consistent in the sense that all models were able to distinguish between low and high velocity sediments within the test area.

The tendency seen in Tab. 5.3 for predictions of higher velocities in the presence of shear waves is notable. However, when the compressional velocity is less than 1600 m/s, the added complexity of shear is hardly justified.

The track 1, 500 Hz, track 3, 0.5 and 4 kHz, and track 4, 4 kHz inversions resulted in practically the same optimal parameter sets for all four models. A contributing factor of the consistency is the small spread at each angle in data.

6 Conclusions

Acoustic propagation in shallow water is influenced by several environmental factors including bathymetry, sound speed and seabed type. The time and space variability of the environment, and the lack of archival information of acoustic parameters in foreign areas, makes it necessary to acquire environmental data from ship underway. This report is focused on rapid determination of geoacoustic parameters by inversion of reflection loss data. The main result is that the velocity of the topmost part of the sediment can be estimated within a computational time of a few seconds. The fast run time implies that the proposed technique is applicable in real-time on data collected on moving platforms, which makes it possible to map large areas with response times comparable to the time for data acquisition.

A basic prerequisite of the inversion of reflection loss data is precise knowledge of the source-receiver geometry and the bathymetry. This study shows how this information can be gained from the probing signals being used for inversion. This is important from an operational point of view as it obviates the need for acoustic positioning systems and the consultation of bathymetry maps.

Four geoacoustic models were tried for the description of the acoustic properties of the sea bottom. The predictions of the sound velocity using these models were consistent in most cases. Further assessments of the relative merits must be based on more extensive measurement.

The inversion of this paper have been concentrated on the sound velocity of the sediment. At the test site the velocity was found to vary in the range 1480 to 1750 m/s with a variability of the order 100 m/s within a distance of a few tens of metres. This information can be extracted rapidly from local measurements of the bottom reflectivity. It remains to see how local estimates of the sound velocity of the sediment can be exploited for predictions of sound propagation at long distance.

In future trials efforts should be made to increase the angular coverage of reflection data. For hard bottoms it is of particular importance to collect reflection data around the critical angle.

In the Rayleigh model the bottom is treated as a plane reflector. In future work proper account should be taken to the effect of scattering losses from surface roughness and volume inhomogeneities beneath the seafloor.

Acknowledgement

We thank CO Jonni Tvinghagen and the crew of HMS Ägir for their assistance in seagoing operations.

We also like to thank Per Morén for sharing his competence on many occassions.

References

[1] R. Sigg and J. Schiöld. COMBIS - version 2.0. Technical report FOI-R–0947–SE, 2003.

[2] B.L. Andersson and P. Morén. Studie av geoakustiska data för sonartaktiskt beslutsstödsystem, UwEM och HAIS-III. Teknisk rapport FOI-R–0448–SE, 2002.

[3] D.G. Simons, M.A. Ainslie, S.H.E. Muller, and W. Boek. RUMBLE Technical Report on Inversion Models. Technical report TD-01-0327; TNO-FEL-02-A132, 2002.

[4] S.H.E. Muller, M.A. Ainslie, W. Boek, and D.G. Simons. Inversion for bottom parameters using low frequency reverberation data. In *Proc. 6th Eur. Conf. Underwater Acoustics, ECUA 2002*, pages 147–152. Gdansk, Poland, 2002.

[5] L. Abrahamsson, E. Dalberg, T. Fristedt, and P. Sigray. Measurements and analysis of sound reflected from the seabed. Technical report FOI-R–1689–SE, 2004.

[6] F. Li, J. Liu, and R. Zhang. A Model/Data comparison for Shallow-Water Reverberation. *IEEE J. Oceanic Eng.*, 29:1060–1066, 2004.

[7] L. Brekhovskikh and Yu. Lysanov. *Fundamentals of Ocean Acoustics.* Springer-Verlag, 1982.

[8] K.L. Williams, E.I. Thorsos, and W.T. Elam. Examination of coherent surface reflection coefficient (CSRC) approximations in shallow water propagation. *J. Acoust. Soc. Amer.*, 116:1975–1984, 2004.

[9] E.I. Thorsos. Acoustic scattering from a "Pierson-Moskowitz" sea surface. *J. Acoust. Soc. Amer.*, 88:335–349, 1990.

[10] B.E. Tucholke. Acoustic environment of the Hatteras and Nares Abyssal Plains, western North Atlantic Ocean, determined from velocities and physical properties of sedeiment cores. *J. Acoust. Soc. Amer.*, 68:1376–1390, 1980.

[11] J.H. Beebe, S.T. McDaniel, and L.A. Rubano. Shallow-water transmission loss predictions using the Biot sediment model. *J. Acoust. Soc. Amer.*, 82:1417–1426, 1982.

[12] H.P. Bucker, J.A. Whitney, G.S. Yee, and R.R. Gardner. Reflection of Low-Frequency Sonar Signals from a Smooth Bottom. *J. Acoust. Soc. Amer.*, 37:1037–1051, 1965.

[13] O.F. Hastrup. Some bottom-reflection loss anomalies near grazing and their effect on propagation in shallow water. In *Bottom-Interacting Ocean Acoustics, ed. W.A Kuperman and F.B. Jensen*, pages 135–152, New York, 1980.

[14] T. Akal and F.B. Jensen. Effects of the Sea-Bed on Acoustic Propagation. In *Acoustics and the Sea-Beds, ed. N.G Pace*, pages 225–232, Bath, UK, 1983.

[15] C.W. Holland. Geoacoustic inversion for fine-grained sediments. *J. Acoust. Soc. Amer.*, 111:1560–1564, 2002.

[16] L. Abrahamsson, B.L. Andersson, I. Karasalo, and P. Sigray. Environment assessment for underwater sensors in the Stockholm archipelago, part 1 - inversion of hydroacoustic sub-bottom parameters. User report FOI-R–0706–SE, 2002.

[17] D. Whitley and T. Starkweather. GENITOR II: a distributed genetic algorithm. *J. Expt. Theor. Artif. Intell.*, 2:189–214, 1990.

[18] N.R. Chapman, J. Desert, A. Agarwal, Y. Stephan, and X. Demoulin. Estimation of seabed models by inversion of broadband acoustic data. In *Proc. 6th Eur. Conf. Underwater Acoustics, ECUA 2002*, pages 477–482. Gdansk, Poland, 2002.